nature materials

ARTICLES

https://doi.org/10.1038/s41563-022-01238-w

Check for updates

Bimorphic Floquet topological insulators

Georgios G. Pyrialakos[1,2,5], Julius Beck[3,5], Matthias Heinrich[3], Lukas J. Maczewsky[3], Nikolaos V. Kantartzis[2], Mercedeh Khajavikhan[4], Alexander Szameit[3] and Demetrios N. Christodoulides[1] ✉

Topological theories have established a unique set of rules that govern the transport properties in a wide variety of wave-mechanical settings. In a marked departure from the established approaches that induce Floquet topological phases by specifically tailored discrete coupling protocols or helical lattice motions, we introduce a class of bimorphic Floquet topological insulators that leverage connective chains with periodically modulated on-site potentials to reveal rich topological features in the system. In exploring a 'chain-driven' generalization of the archetypical Floquet honeycomb lattice, we identify a rich phase structure that can host multiple non-trivial topological phases associated simultaneously with both Chern-type and anomalous chiral states. Experiments carried out in photonic waveguide lattices reveal a strongly confined helical edge state that, owing to its origin in bulk flat bands, can be set into motion in a topologically protected fashion, or halted at will, without compromising its adherence to individual lattice sites.

Floquet engineering provides a powerful tool for shaping the topological structure of fermionic and bosonic settings alike[1–12]. At its core, it relies on the fact that a proper periodic modulation can induce chirality to arrangements of non-interacting particles, thereby giving rise to a wide range of topological insulators (TIs). Under these conditions, symmetry-protected states emerge along the boundaries of a modulated lattice, allowing for scatter-free transport on edges or interfaces with static (topologically trivial) domains. As such, helical transport constitutes a hallmark signature of complex topological order, and its presence in Floquet-driven systems highlights how periodic modulations can systematically extend the original classification of topological phases[13–19] beyond static systems with spin–orbit coupling or magnetic order. Along these lines, different topological invariants such as the winding number[20] are required to describe the topological nature of gaps with vanishing Chern numbers $\mathcal{C}=0$ (refs. [21–23]). These new degrees of freedom have enabled the experimental realization of a wide variety of topological systems in photonic lattices, ranging from anomalous Floquet TIs[1–3] to systems exhibiting Weyl point dynamics[24], Anderson TIs[25], TIs in synthetic dimensions[26], photonic $\mathbb{Z}_2$ TIs exhibiting fermionic time-reversal symmetry[27] and topological lasers[28]. Quite recently, anomalous driving protocols have enabled the observation of solitons in topological bandgaps[29], the creation of nonlinearity-induced TIs[30] and investigations into the nonlinear dynamics of higher-order topological insulators[31].

Historically, photonic waveguide Floquet insulators can be divided into two distinct categories according to the character of the modulation involved. The first class is based on diatomic lattices (Fig. 1a), whereby a topological regime may be brought about by helical trajectories of the individual waveguide sites (Fig. 1b), introducing an effective chiral gauge field and, in turn, a non-trivial Chern insulating phase to the system[4]. On the other hand, more complex Floquet phases can be synthesized by step-wise coupling protocols that periodically allow for the selective interaction between neighbouring sites (along different lattice vectors) by varying their corresponding separations (Fig. 1c)[1,2]. Approaching the synthesis of topological phases from two opposite directions, namely discrete coupling steps as opposed to the effective-medium strategy of rapidly spiralling waveguides, these two regimes would appear to be mutually exclusive. In this work, we introduce a third paradigm that embodies the distinctive characteristics of both aforementioned classes while overcoming their most pressing physical constraints. To this end, we introduce interstitial elements[32] between the sites of a static periodic lattice that act as Floquet drivers for the system (Fig. 1d). In doing so, these sites allow us to leverage the periodic modulation of their on-site potentials in order to synthesize hybrid topological systems whose band structure simultaneously hosts both conventional Chern insulator bands ($\mathcal{C}=1$) and anomalous topological bands ($\mathcal{C}=0$), and is even capable of supporting topological phases with higher ranked invariants ($\mathcal{C}=2$), in lattices with z-invariant site positions.

Floquet potentials in a chained honeycomb lattice. To exemplify our approach, let us consider a honeycomb lattice of weakly coupled elements, in which the three nearest-neighbour couplings vary independently in a cyclic fashion along the time (or propagation) coordinate. Despite a vanishing Chern number $\mathcal{C}=0$, such arrangements are known to be capable of supporting different insulating and non-trivial Floquet topological phases[10]. The topological properties of this anomalous system are characterized by a three-dimensional winding number $\mathcal{W}$, which considers the temporal evolution of the system and counts the edge states that cross a particular bandgap[20]. The Chern number of any band can be associated with the difference between the adjacent gaps' winding numbers, $\mathcal{C}=\mathcal{W}_{\text{above}}-\mathcal{W}_{\text{below}}$ (refs. [20,21]). A spatially fixed implementation of a non-trivial Floquet phase is forbidden by the symmetry rules of a diatomic lattice. In other words, no conceivable modulation of their two on-site potentials is capable of imbuing the Hamiltonian with helicity. In addition, any imbalance between the potentials inadvertently breaks the sublattice symmetry, and

[1]College of Optics & Photonics-CREOL, University of Central Florida, Orlando, FL, USA. [2]Department of Electrical and Computer Engineering, Aristotle University of Thessaloniki, Thessaloniki, Greece. [3]Institute for Physics, University of Rostock, Rostock, Germany. [4]Ming Hsieh Department of Electrical and Computer Engineering, University of Southern California, Los Angeles, CA, USA. [5]These authors contributed equally: Georgios G. Pyrialakos, Julius Beck. ✉e-mail: demetri@creol.ucf.edu

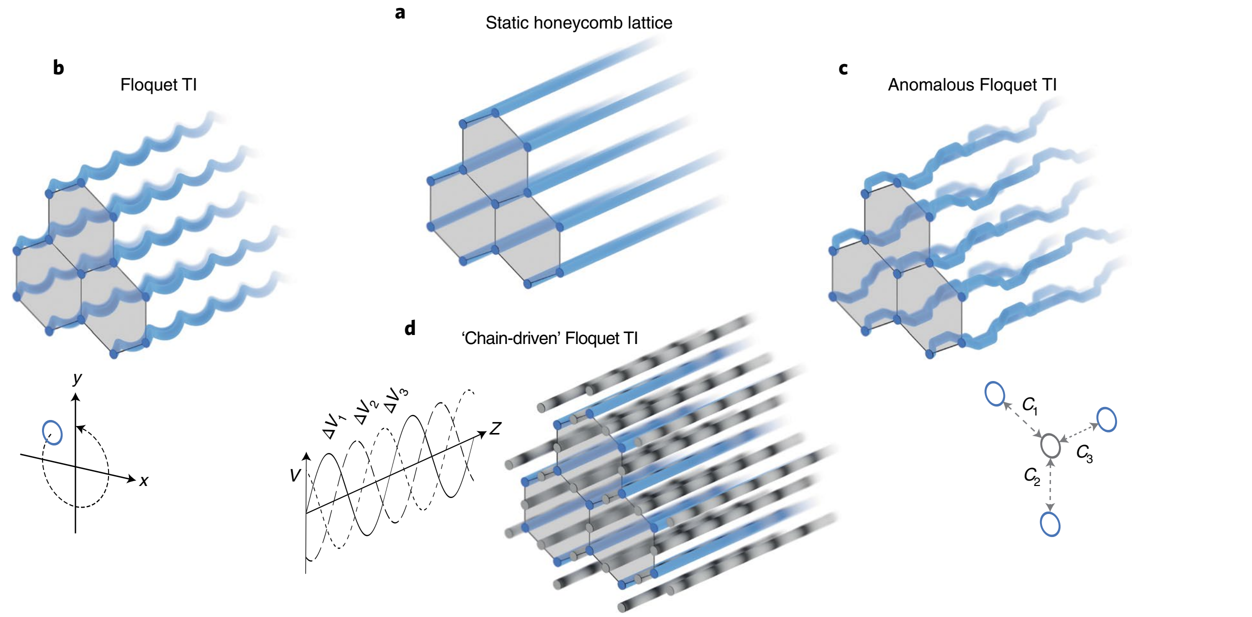

Fig. 1 | A new road to topological lattices. a, In the absence of magnetic interactions, periodic systems such as the honeycomb lattice in **a** can be rendered topologically non-trivial by appropriate periodic modulations. **b**, Conventional Floquet TIs achieve this by inducing a virtual magnetic flux via a global helical motion of the entire lattice, yielding a Chern-type topological phase. **c**, Anomalous Floquet TIs instead are based on multistep driving protocols that impose helicity by independently modulating the coupling strengths *c* between specific neighbours. Their topological properties are characterized by a winding number. Despite their different physical mechanisms, both of these approaches involve continual dynamic changes to the positions of the individual lattice sites—the main source of losses in Floquet waveguide systems. **d**, The 'chain-driven' Floquet TIs presented here instead leverage connective interstitial elements whose on-site potentials ΔV are modulated in a cyclical fashion. Such systems offer rich topological phases that simultaneously support both Chern-type and anomalous topological states in a geometrically static arrangement.

in turn introduces a trivial bandgap that prevents the topological transition.

To overcome these limitations, we introduce interstitial elements between the main sites of the potential lattice, one in each coupling path between adjacent sites of the two sublattices. Figure 2 illustrates how the band structure of the honeycomb system (Fig. 2a) is altered in the presence of these interstitial sites (Fig. 2b). Two copies of the honeycomb spectrum (Fig. 2a), each of which features a pair of Dirac cones in the first Brillouin zone, coexist symmetrically around multiple degenerate flat bands located at zero energy. The latter are composed of compact localized states that reside exclusively within the chain elements, locked by the destructive interference of light at the main sites. This particular modal structure is supported by the presence of additional symmetries in a system that hosts an odd total number of fundamental eigenmodes[33,34], here originating from the 5×5 bulk Hamiltonian

$$\begin{aligned} H(\mathbf{k}) &= \sum_{j=1}^{3}\beta_j(t)\psi_j^\dagger\psi_j \\ &+\sum_{j=1}^{3}c_j\,(t)\left(\psi_j^\dagger\psi_\mathrm{A}\mathrm{e}^{i\mathbf{k}\cdot\boldsymbol{\delta}_{j\mathrm{A}}}+\psi_j^\dagger\psi_\mathrm{B}\mathrm{e}^{i\mathbf{k}\cdot\boldsymbol{\delta}_{j\mathrm{B}}}\right)+\mathrm{h.c.} \end{aligned} \tag{1}$$

where $\mathbf{k}$ is the Bloch vector momentum, t is the time variable, $\psi^\dagger$ and ψ are the creation and annihilation operators on the lattice sites and $\boldsymbol{\delta}_{j\mathrm{A}}$ and $\boldsymbol{\delta}_{j\mathrm{B}}$ are lattice vector displacements between the jth chain element and the main site of sublattices A and B, respectively. Here, h.c. stands for the Hermitian conjugate. Out of the fifteen independent terms of the Hermitian Hamiltonian, only nine remain in equation (1), six involving nearest-neighbour interactions (with couplings c_1, c_2 and c_3) and three involving on-site potential shifts exclusively at the interstitial sites ($\beta_1, \beta_2, \beta_3 \neq 0$; $\beta_\mathrm{A}, \beta_\mathrm{B} = 0$). Each of these terms can be addressed independently without perturbing the balance between sites A and B, thus fully preserving sublattice symmetry in the unit cell. In a continuous representation of the system (that is, the Schrödinger equation with a continuous refractive index profile), the time variation of both c_j and β_j can be realized via modification of the potential contrast at the interstitial sites—in other words, it is specifically these sites that can be leveraged to bring about a topological phase transition.

We consider how the system responds under sinusoidal modulations that are chirally phase-shifted by $2\pi/3$ between the three interstitial sites surrounding each primary site. In this case, the potential at the site between elements A and B of the jth chain is given by $V_j(t) = 1 + \sin(2\pi t/T + 2\pi j/3)$, where $j \in \{1,2,3\}$ and T denotes the Floquet period. Note that, by using an effective 2×2 tight-binding representation of the system (Supplementary Section I), this is equivalent to a continuous helical rotation of the principal direction of maximal coupling, despite the spatially static arrangement of the lattice sites. The topological changes due to the periodic drive can be traced by means of the unitary $\mathbf{k}$-space evolution operator

$$U(\mathbf{k},t) = \mathcal{T}\exp\left(-i\int_0^t \mathrm{d}t' H(\mathbf{k},t')\right)$$

where $\mathcal{T}$ denotes time-ordering and H corresponds to the time-dependent Hamiltonian integrated over time t'. In this respect, we decompose $U = U_\mathrm{s}U_\mathrm{d}$ into a product of a quasi-static term $U_\mathrm{s} = \exp(-iH_\mathrm{eff}t)$ with $H_\mathrm{eff} = i/T\log(U(\mathbf{k},T))$ and a dynamic term U_d that accounts for the periodic micro-motion of the mode during the period of the drive with $U_\mathrm{d}(\mathbf{k},T) = \mathbb{I}$ the identity operator[35]. Note that the effective Hamiltonian conforms to the traditional ten-fold way classification[15], which, in this two-dimensional setting, is characterized by a $\mathbb{Z}$ topological invariant. As depicted in the example of Fig. 2c, for a Floquet period of $T = 2\pi/7$, the quasi-energy

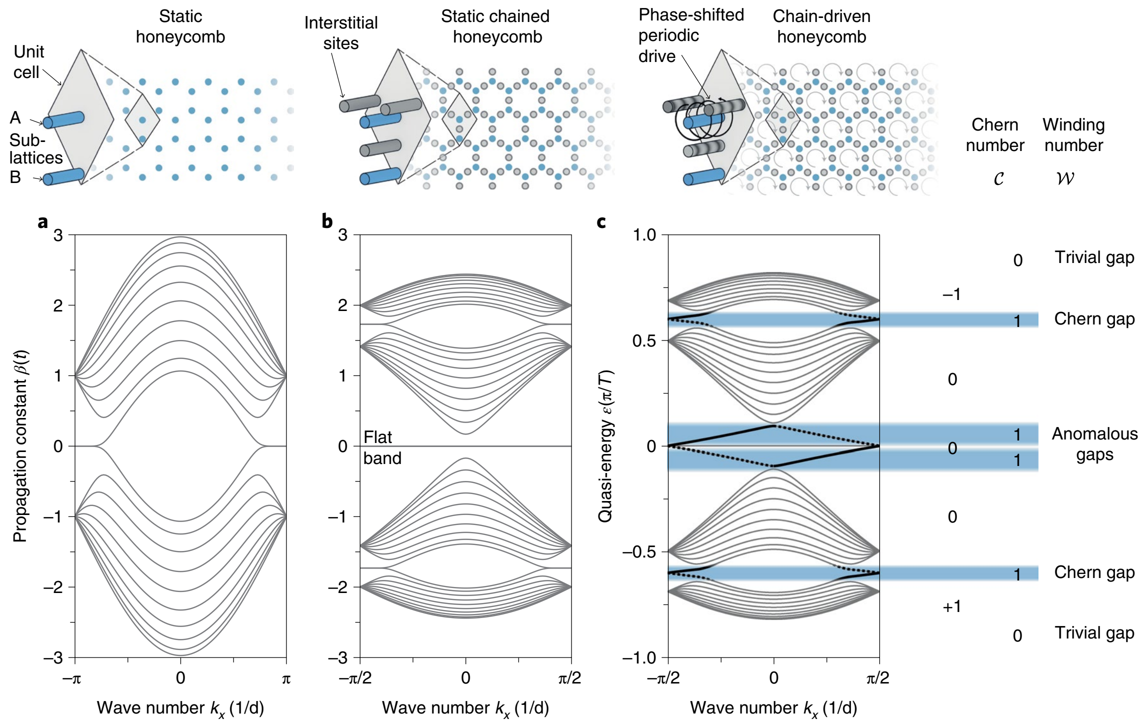

Fig. 2 | Band structures and topological characterization. a, The zigzag-terminated edges of a conventional static honeycomb lattice support edge states that emerge from the Dirac points and extend towards the boundaries of the first Brillouin zone. **b**, A static chained honeycomb lattice is obtained by introducing interstitial elements between each adjacent pair of principal sites. The resulting band structure manifests multiple degenerate flat-band states that are interposed between two copies of the diatomic spectrum. **c**, A chain-driven honeycomb lattice. By modulating the on-site potential of the interstitial sites in a sinusoidal fashion with clockwise-rotating relative phases, a total of four gaps open in the bulk, as indicated by the light grey shading. The edges support four pairs of helical states (thick lines), one for each topological gap. In all band structure diagrams, the wave number is expressed in terms of the inverse unit cell size *d*. The values of the Chern ($\mathcal{C}$) and winding ($\mathcal{W}$) invariants, marked on the right, reveal the topological nature of each bandgap. Notably, the edge states that emerge from the flat band resemble an anomalous topological phase, characterized by a non-trivial winding number ($\mathcal{W}=1$) and a trivial Chern invariant ($\mathcal{C}=0$). Details on the modal amplitudes of the Chern states in the $\mathcal{C}=1$ phase are provided in Supplementary Fig. 4.

spectrum $\varepsilon(\mathbf{k})$ of H_{eff} exhibits $\mathcal{C}=1$ in the upper- and lowermost bands, indicating the formation of a pair of Chern-type topological bandgaps around the Dirac points. In turn, these gaps support helical edge states on the zigzag edge similar to the ones in a conventional photonic Floquet TI[4]. At the same time, however, the action of the periodic chain drive opens another gap around $\varepsilon=0$. Being nested between bulk bands with $\mathcal{C}=0$, its anomalous topological nature is revealed only by the value of the winding number, that is $\mathcal{W}=1$. While the topological edge states traversing this gap with constant slope are likewise helical, they inherit a key characteristic of the zero-energy flat band that they emerge from: the power in these states exclusively resides within the three interstitial sites of the edge unit cells (Supplementary Fig. 3). Finally, the remaining degenerate flat band at $\varepsilon=0$ shows that the quasi-energies of the chained lattice's bulk compact localized states remain on average unaffected by the presence of the periodic modulation; that is, the self-locking property of the flat-band modes clearly survives the topological phase transition. As a result, these bimorphic chain-driven lattices can both host compact localized states in the bulk and provide virtually dispersion-free mobility for tightly confined wave packets along the edge.

Observation of topological compact localized states. To experimentally probe the propagation dynamics of the different topological states in chain-driven lattices, we employ femtosecond laser direct-written photonic lattices[36] as a platform for their implementation (Methods). The evolution of light in such systems is governed by a Schrödinger equation in which the propagation coordinate z represents time and the refractive index profiles of the individual waveguides act as interacting potential wells. In this context, the effective refractive index Δn^{eff} of each waveguide provides direct control over the on-site potential and can be seamlessly tuned by modulating the inscription velocity along the propagation coordinate z. In turn, evanescent coupling between adjacent waveguides instantiates the required hopping terms. Having confirmed numerically that the desired characteristics of the 5×5 tight-binding model can be faithfully reproduced (Supplementary Section II) within the experimentally accessible parameter range of our platform, we fabricated triangular chain-driven lattices composed of 42 unit cells (Fig. 3a). Despite its decidedly bristly appearance, the lattice is in fact terminated by the chained generalization of three zigzag-type edges, since the outermost waveguides represent interstitial sites. In a first set of experiments, we targeted the dispersive Chern states in the vicinity of the Dirac points by synthesizing a spectrally narrow wave packet of an appropriate wave vector via a tripartite excitation pattern with alternating phases injected into three consecutive primary sites along the vertical edge of the system. A series of measurements for different initial positions (Fig. 3c) clearly shows a systematic counterclockwise transport that is confirmed by extended-range numerical simulations (Fig. 3d) and allows light to circumnavigate the corners of the waveguide array. By contrast, when the alternating phase is removed from the excitation pattern, strong bulk diffraction was observed (Extended Data Fig. 1), highlighting the absence

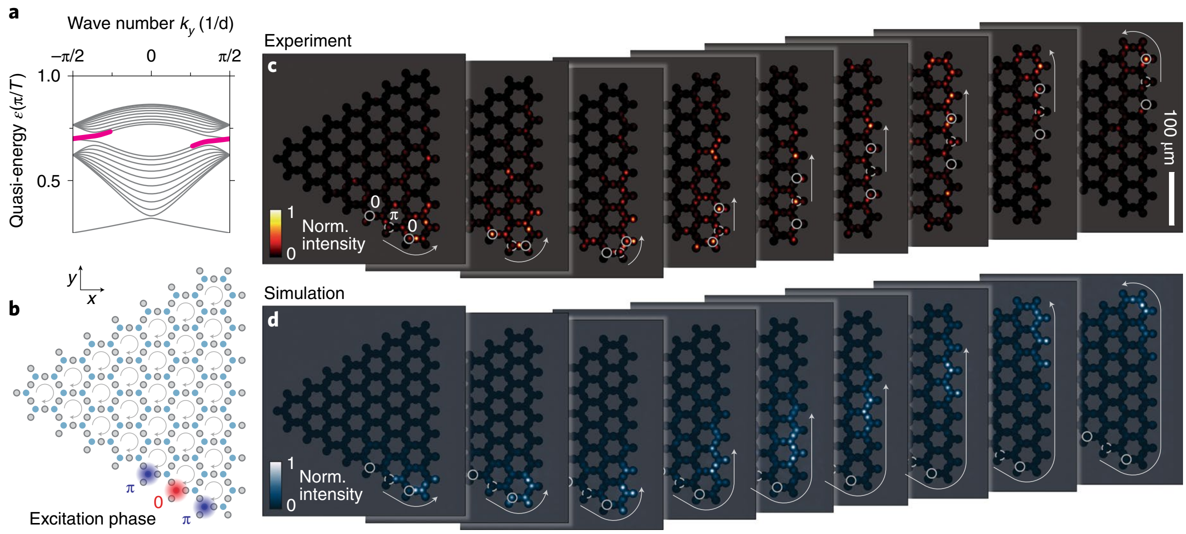

Fig. 3 | Probing the Chern edge state of a photonic chain-driven honeycomb lattice. a,**b**, In order to selectively populate the topological state supported by the Chern gap, indicated by thick magenta branches in the ribbon band structure plot (**a**), three consecutive primary sites along the zigzag edge are excited with identical amplitudes but alternating phases, synthesizing a spectrally narrow wave packet at the edge of the Brillouin zone (**b**). **c**, Experimentally observed output intensity patterns at 633 nm after a propagation length of 150 mm for various placements of the initial excitation along the edge of the lattice; positions and phase are shown by solid (phase 0) and dashed (phase π) white circles. As a guide to the eye, the outlines of the respective lattice are indicated by a semi-transparent overlay. The white arrows indicate the propagation path of the wavepacket from its initial injection site. Norm., normalized. **d**, As confirmed by extended-range beam-propagation method simulations shown for consecutive multiples of the sample length, starting from the lowest three unit cells of the lower diagonal, a substantial fraction of the launched light is captured by the topological Chern mode and transported around the lower corner and up along the vertical edge in a counterclockwise fashion. By comparison, the experimental and numerical results for equivalent flat-phase excitations along the vertical edge are shown in Extended Data Fig. 1. Without the staggered phase, light inevitably diffracts freely across the entire lattice.

of the Chern state in the centre of the Brillouin zone (at Bloch momenta $k_{x,y} \approx 0$).

Owing to their flat-band origins and Brillouin-zone-spanning nature (Fig. 4a), the anomalous topological edge states of the chain-driven lattice can be readily populated by injecting light into individual outermost interstitial sites. In a second set of experiments, we therefore traced the propagation of such single-site excitations along the edge and around two corners of the system (Fig. 4b), and observed helical topological transport in a counterclockwise direction that, in contrast to the dispersive Chern channel, maintains the narrow width of the edge wave packet. This behaviour is also confirmed by numerical extended-range propagation simulations (Fig. 4c). Single-site excitations of bulk interstitial sites instead remain localized at their initial positions (Fig. 4d,e) as dictated by the quasi-static part U_q of the evolution operator, despite the fact that the dynamic part U_d intermittently allows light to enter the neighbouring sites during each Floquet cycle. Comparing these results to the discrete diffraction in a reference lattice of identical geometry implemented without the periodic modulation, we find that light injected into the interstitial sites on the edge as well as within the bulk of the non-driven lattice remains localized by virtue of the flat-band states residing there (Fig. 4f–j). This complementary behaviour opens up the possibility of imprinting arbitrary excitation patterns in the edge channels of chain-driven Floquet TIs. The fact that the Floquet drive can be temporarily frozen and resumed at will without any changes to the lattice geometry provides exceptional control over their topological transport dynamics: once synthesized, compact wave packets can propagate along the edge without being subjected to dispersive broadening, while the unique properties of the flat band allow them to be freely shifted between travelling and localized states without ever rendering them vulnerable to bulk diffraction (Supplementary Video 1).

Discussion

Notably, the chained lattice exhibits a number of higher-order topological phases that may occur for alternate periods of the drive. Changing the period T of the modulation, in relation to the scale given by the inverse coupling in the system, allows adjacent unit cells of the $2\pi/T$-periodic quasi-energy spectrum to overlap in a topologically non-trivial fashion. In the conventional coupling-modulated honeycomb system, a critical period $T_C = \pi/3$ separates the Chern phase ($\mathcal{C} = \pm 1$ and $\mathcal{W} = 0$ for $T > T_C$) and the anomalous phase ($\mathcal{C} = 0$ and $\mathcal{W} = 1$ for $T < T_C$), as illustrated in Extended Data Fig. 2. By contrast, the upper- and lowermost bands of the chain-driven lattice exhibit $|\mathcal{C}| > 1$ for any finite value of T, allowing for the Chern-type and anomalous regimes to naturally coexist and interact in new and interesting ways: as T is increased above a new critical point $T'_C = \pi > T_C$, the bands closer to zero energy enter a higher-order Chern phase ($\mathcal{C} = \pm 2$) as additional pairs of topological edge states emerge in their neighbouring gaps (Extended Data Fig. 3 and Supplementary Fig. 5).

In this work, we proposed and experimentally demonstrated a bimorphic class of Floquet TIs based on periodic modulations of certain on-site potentials. We showed how a 'chained' honeycomb lattice, in which the exchange of population between primary sites is mediated by interstitial sites, can be endowed with rich topological features without resorting to magnetic interactions, helical lattice motion[4] or complex coupling protocols[1,2]. Beyond providing a complementary route towards inducing topology, our 'chain-driven' systems synergistically combine the characteristic features of conventional and anomalous Floquet TIs, allowing for the simultaneous existence of Chern-type chiral states and transport without dispersion in quasi-localized wave packets. These anomalous modes bifurcate from the flat band of the static system and, as such, can be readily converted into their likewise topologically protected,

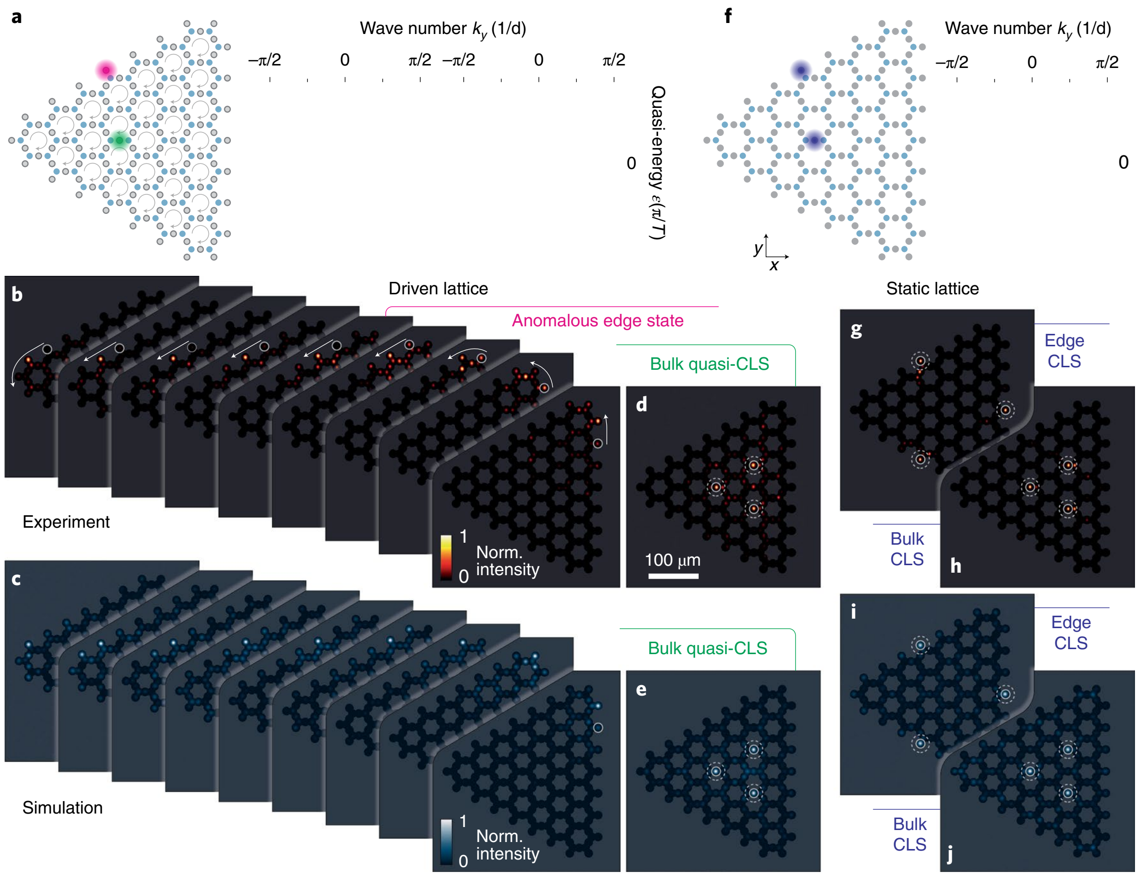

Fig. 4 | Anomalous edge-state propagation and compact localized bulk states. a, In contrast to the Chern modes, the flat-band-derived modes can be efficiently populated by single-waveguide excitations of the interstitial sites along the edge. **b**, Experimentally observed output intensity patterns after a propagation length of 150 mm for various placements of the initial excitation along the edge of the chain-driven lattice. The injection positions are indicated by white circles (solid and dashed for 0 and π phase, respectively). As a guide to the eye, the outlines of the respective lattice are indicated by a semi-transparent overlay. The white arrows indicate the propagation path of the wavepacket from its initial injection site. **c**, As confirmed by extended-range beam-propagation method simulations shown for consecutive multiples of the sample length, a substantial fraction of the launched light is captured by the anomalous topological mode and transported along the edge in a counterclockwise fashion. **d**,**e**, Within the bulk of the chain-driven lattice, light injected into the interstitial sites remains trapped in the quasi-compact localized states (quasi-CLS) and only undergoes a small degree of micro-motion during each Floquet period. **f**–**j**, The degenerate flat band of the non-driven chained honeycomb lattice is composed of compact localized states residing on the interstitial sites in the bulk as well as along the edge.

compact localized counterparts. While our findings are general and can be readily adapted to any topological platform that offers the means to dynamically control the on-site potential, such as cold atoms[37], electronic circuits[38] or even mechanics[39], the capability to affect topological phase transitions without changes to the lattice geometry is of particular importance in the context of topological photonics, where curved waveguide trajectories inevitably entail additional losses. Moreover, it paves the way towards sophisticated designs involving several coexisting modulation periods and even regions with opposite helicity that can seamlessly interact without associated local coupling defects that would be inevitable in systems with modulated waveguide trajectories. Along these lines, we envision a new generation of low-loss robust photonic circuitry in which optically encoded packets of information can be transported, steered and even reshuffled without compromising their topological protection at any point.

Online content

Any methods, additional references, Nature Research reporting summaries, source data, extended data, supplementary information, acknowledgements, peer review information; details of author contributions and competing interests; and statements of data and code availability are available at https://doi.org/10.1038/s41563-022-01238-w.

Received: 9 September 2021; Accepted: 18 March 2022;
Published online: 28 April 2022

References

1. Maczewsky, L. J. et al. Observation of photonic anomalous Floquet topological insulators. *Nat. Commun.* **8**, 13756 (2017).
2. Mukherjee, S. et al. Experimental observation of anomalous topological edge modes in a slowly driven photonic lattice. *Nat. Commun.* **8**, 13918 (2017).
3. McIver, J. W. et al. Light-induced anomalous Hall effect in graphene. *Nat. Phys.* **16**, 1058–1063 (2020).
4. Rechtsman, M. C. et al. Photonic Floquet topological insulators. *Nature* **496**, 196–200 (2013).
5. Aidelsburger, M. et al. Experimental realization of strong effective magnetic fields in an optical lattice. *Phys. Rev. Lett.* **107**, 255301 (2011).
6. Liu, G., Hao, N., Zhu, S.-L. & Liu, W. M. Topological superfluid transition induced by a periodically driven optical lattice. *Phys. Rev. A* **86**, 013639 (2012).
7. Nathan, F., Abanin, D., Berg, E., Lindner, N. H. & Rudner, M. S. Anomalous Floquet insulators. *Phys. Rev. B* **99**, 195133 (2019).
8. Hafezi, M. et al. Imaging topological edge states in silicon photonics. *Nat. Photon.* **7**, 1001–1005 (2013).

9. Sie, E. J. et al. Valley-selective optical Stark effect in monolayer WS_2. *Nat. Mater.* **14**, 290–294 (2015).
10. Cooper, N. R., Dalibard, J. & Spielman, I. B. Topological bands for ultracold atoms. *Rev. Mod. Phys.* **91**, 015005 (2019).
11. Wintersperger, K. et al. Realization of an anomalous Floquet topological system with ultracold atoms. *Nat. Phys.* **16**, 1058–1063 (2020).
12. Peng, Y.-G. et al. Experimental demonstration of anomalous Floquet topological insulator for sound. *Nat. Commun*. **7**, 13368 (2016).
13. Nathan, F. & Rudner, M. S. Topological singularities and the general classification of Floquet–Bloch systems. *New J. Phys.* **17**, 125014 (2015).
14. Chiu, C.-K., Teo, J. C. Y., Schnyder, A. P. & Ryu, S. Classification of topological quantum matter with symmetries. *Rev. Mod. Phys.* **88**, 035005 (2016).
15. Roy, R. & Harper, F. Periodic table for Floquet topological insulators. *Phys. Rev. B* **96**, 155118 (2017).
16. Wang, C., Zhang, P., Chen, X., Yu, J. & Zhai, H. Scheme to measure the topological number of a Chern insulator from quench dynamics. *Phys. Rev. Lett.* **118**, 185701 (2017).
17. Tarnowski, M. et al. Measuring topology from dynamics by obtaining the Chern number from a linking number. *Nat. Commun.* **10**, 1728 (2019).
18. Ünal, F. N., Eckardt, A. & Slager, R.-J. Hopf characterization of two-dimensional Floquet topological insulators. *Phys. Rev. Res.* **1**, 022003(R) (2019).
19. Schuster, T., Gazit, S., Moore, J. E. & Yao, N. Y. Floquet Hopf insulators. *Phys. Rev. Lett.* **123**, 266803 (2019).
20. Rudner, M. S., Lindner, N. H., Berg, E. & Levin, M. Anomalous edge states and the bulk-edge correspondence for periodically driven two-dimensional systems. *Phys. Rev. X* **3**, 031005 (2013).
21. Kitagawa, T., Berg, E., Rudner, M. & Demler, E. Topological characterization of periodically driven quantum systems. *Phys. Rev. B* **82**, 235114 (2010).
22. Nathan, F. & Rudner, M. S. Topological singularities and the general classification of Floquet–Bloch systems. *New J. Phys.* **17**, 125014 (2015).
23. Carpentier, D. et al. Topological index for periodically driven time-reversal invariant 2D systems. *Phys. Rev. Lett.* **114**, 106806 (2015).
24. Noh, J. et al. Experimental observation of optical Weyl points and Fermi arc-like surface states. *Nat. Phys.* **13**, 611–617 (2017).
25. Stützer, S. et al. Photonic topological Anderson insulators. *Nature* **560**, 461–465 (2018).
26. Lustig, E. et al. Photonic topological insulator in synthetic dimensions. *Nature* **567**, 356–360 (2019).
27. Maczewsky, L. J. et al. Fermionic time-reversal symmetry in a photonic topological insulator. *Nat. Mater.* **19**, 855–860 (2020).
28. Bandres, M. A. et al. Topological insulator laser: experiments. *Science* **359**, eaar4005 (2018).
29. Mukherjee, S. & Rechtsman, M. C. Observation of Floquet solitons in a topological bandgap. *Science* **368**, 856–859 (2020).
30. Maczewsky, L. J. et al. Nonlinearity-induced photonic topological insulator. *Science* **370**, 701–704 (2020).
31. Kirsch, M. et al. Nonlinear second-order photonic topological insulators. *Nat. Phys*. https://doi.org/10.1038/s41567-021-01275-3 (2021).
32. Pyrialakos, G. et al. Symmetry-controlled edge states in the type-II phase of Dirac photonic lattices. *Nat. Commun.* **11**, 2074 (2020).
33. Ramachandran, A., Andreanov, A. & Flach, S. Chiral flat bands: existence, engineering, and stability. *Phys. Rev. B* **96**, 161104(R) (2017).
34. Xia, S. et al. Unconventional flatband line states in photonic Lieb lattices. *Phys. Rev. Lett.* **121**, 263902 (2018).
35. Goldman, N. & Dalibard, J. Periodically driven quantum systems: effective Hamiltonians and engineered gauge fields. *Phys. Rev. X* **4**, 031027 (2014).
36. Szameit, A. & Nolte, S. Discrete optics in femtosecond-laser-written photonic structures. *J. Phys. B* **43**, 163001 (2010).
37. Jotzu, G. et al. Experimental realization of the topological Haldane model with ultracold fermions. *Nature* **515**, 237–240 (2014).
38. Hadad, Y. et al. Self-induced topological protection in nonlinear circuit arrays. *Nat. Electron.* **1**, 178–182 (2018).
39. Süsstrunk, R. & Huber, S. D. Observation of phononic helical edge states in a mechanical topological insulator. *Science* **349**, 47–50 (2015).

Methods

Experimental configuration. The photonic structures used in our experiments are inscribed by focusing ultrashort laser pulses from a frequency-doubled fibre amplifier system (Coherent Monaco, wavelength 517 nm, repetition rate 333 kHz, pulse duration 270 fs) into the volume of a fused silica sample (Corning 7980, dimensions 1 mm × 20 mm × 150 mm, bulk refractive index $n_0 = 1.457$ at 633 nm), inducing permanent refractive index changes along arbitrary three-dimensional trajectories as defined by the motion of a precision translation system (Aerotech ALS130). Due to the focusing conditions, these waveguides exhibit slightly elliptical mode fields with a typical refractive index contrast of up to $\Delta n_0 = 2 \times 10^{-3}$. The selective modulation of the interstitial sites' index in a range of ±10% around this value was achieved by an appropriate modulation of the inscription speed between 92 and 156 mm min^{-1}. The ideal profile of the sinusoidal index modulation was approximated by twelve constant-index segments per Floquet period. Waveguide fluorescence imaging[40] shows that even for such a relatively coarse discretization, the modulated channels exhibit excess losses of only 0.096 ± 0.010 dB cm^{-1} relative to the static waveguides (compare with Extended Data Fig. 4). With half of the lattice sites being modulated, the mean excess losses of the bimorphic Floquet TI are 0.048 ± 0.005 dB cm^{-1}, substantially below the 1.7 dB cm^{-1} of bending losses reported for conventional Floquet TIs based on helically modulated waveguides[4]. The topological propagation dynamics were probed with coherent light from a tuneable supercontinuum source (NKT SuperK Extreme), allowing us to compensate for the micro-motion of the wave packets within the Floquet period and faithfully capture the dynamics according to the quasi-static evolution operator by varying the excitation wavelength between 570 nm and 633 nm. The appropriate intensity and phase distributions for the desired excitation conditions were synthesized with a spatial light modulator (Hamamatsu LCOS-SLM).

Numerical simulations. The numerical results are obtained by solving the paraxial Schrödinger equation as an eigenvalue problem (for computations of the band structure, via the finite-difference method) and as a propagation problem (for computations of the field dynamics, via the beam-propagation method). In this context, the ribbon band diagrams of Figs. 2 and 3 provide the necessary validation for the tight-binding chain approximation. The robustness of the chiral transport against a variety of defects was verified by beam-propagation method simulations (Supplementary Fig. 6).

To efficiently reduce the computational burden of the time-dependent eigenvalue problem, we decompose the solution space into a sinusoidal basis along the propagation axis. This approach relies on the expectation that the time-periodic part of the eigenmode solution will be related to the driving protocol used for the time-dependent modulation of the refractive index. This strategy leads into a solution space that is numerically large in the transverse plane (discretized by finite differences) but highly reduced along the z dimension. The size of the matrix generated through this process is optimally minimized so that it remains within reach of common eigenvalue decomposing techniques. More information is in Supplementary Section II.

Reporting Summary. Further information on research design is available in the Nature Research Reporting Summary linked to this article.

Data availability

The experimental data that support the findings of this study are available from M.H. upon reasonable request (matthias.heinrich@uni-rostock.de).

Code availability

The MATLAB codes corresponding to the beam-propagation method and band structure algorithms are available from G.G.P. upon reasonable request (pyrialak@knights.ucf.edu).

References

40. Szameit, A. et al. Quasi-incoherent propagation in waveguide arrays. *Appl. Phys. Lett.* **90**, 241113 (2007).

Acknowledgements

We thank C. Otto for preparing the high-quality fused silica samples used for the inscription of all photonic structures employed in the experiments presented here. G.G.P. acknowledges the support of the Bodossaki Foundation. This work was partially supported by Defense Advanced Research Projects Agency (DARPA; D18AP00058), Office of Naval Research (ONR) Multidisciplinary University Research Initiative (MURI; N00014-16-1-2640, N00014-18-1-2347, N00014-19-1-2052, N00014-20-1-2522, N00014-20-1-2789), Air Force Office of Scientific Research (AFOSR MURI; FA9550-20-1-0322, FA9550-21-1-0202), the National Science Foundation (DMR-1420620, EECS-1711230, ECCS-1454531, DMR-1420620, ECCS-1757025, CBET-1805200, ECCS-2000538, ECCS-2011171), Mathematics and Physical Sciences (MPS) Simons collaboration (Simons grant 733682), W. M. Keck Foundation, US–Israel Binational Science Foundation (BSF 2016381) and the US Air Force Research Laboratory (FA9550-14-1-0037, FA9550-20-1-0322, FA9550-21-1-0202, FA86511820019). We furthermore acknowledge funding from the Deutsche Forschungsgemeinschaft (SCHE 612/6-1, SZ 276/12-1, BL 574/13-1, SZ 276/15-1, SZ 276/20-1) and the Alfried Krupp von Bohlen and Halbach Foundation.

Author contributions

G.G.P. initiated the idea, formulated the index-modulated lattice and performed the theoretical calculations and simulations. J.B. developed the experimental implementation, fabricated the samples and conducted the measurements. J.B., L.J.M. and M.H. evaluated the measurements and interpreted the data. M.K., N.V.K., A.S. and D.N.C. supervised the efforts of their respective groups. All authors discussed the results and cowrote the manuscript.

Competing interests

The authors declare no competing interests.

Additional information

Extended data is available for this paper at https://doi.org/10.1038/s41563-022-01238-w.

Supplementary information The online version contains supplementary material available at https://doi.org/10.1038/s41563-022-01238-w.

Correspondence and requests for materials should be addressed to Demetrios N. Christodoulides.

Peer review information *Nature Materials* thanks Alexander Khanikaev, Sunil Mittal and the other, anonymous, reviewer(s) for their contribution to the peer review of this work.

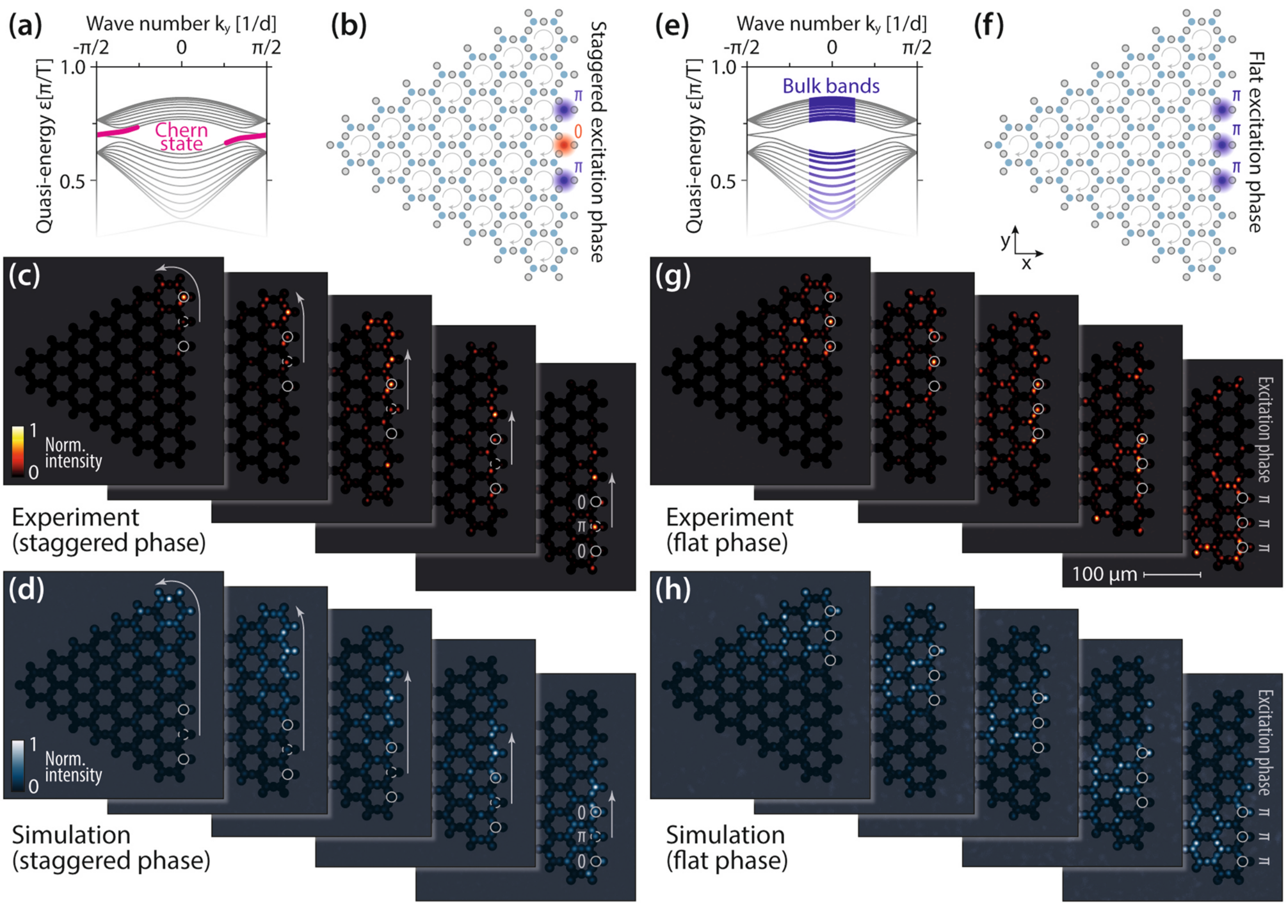

Extended Data Fig. 1 | Comparison of staggered and flat-phased broad excitations. (a-d): Staggered excitations of the primary waveguides of edge unit cells successfully populate the topological Chern mode near the edge of the Brillouin zone. (e-h) Absent the appropriate phase modulation, the injected wave packets instead represent a superposition of the bulk bands near the center of the Brillouin zone. As a result, the light diffracts freely across the entire lattice instead of being captured in the helical Chern channel.

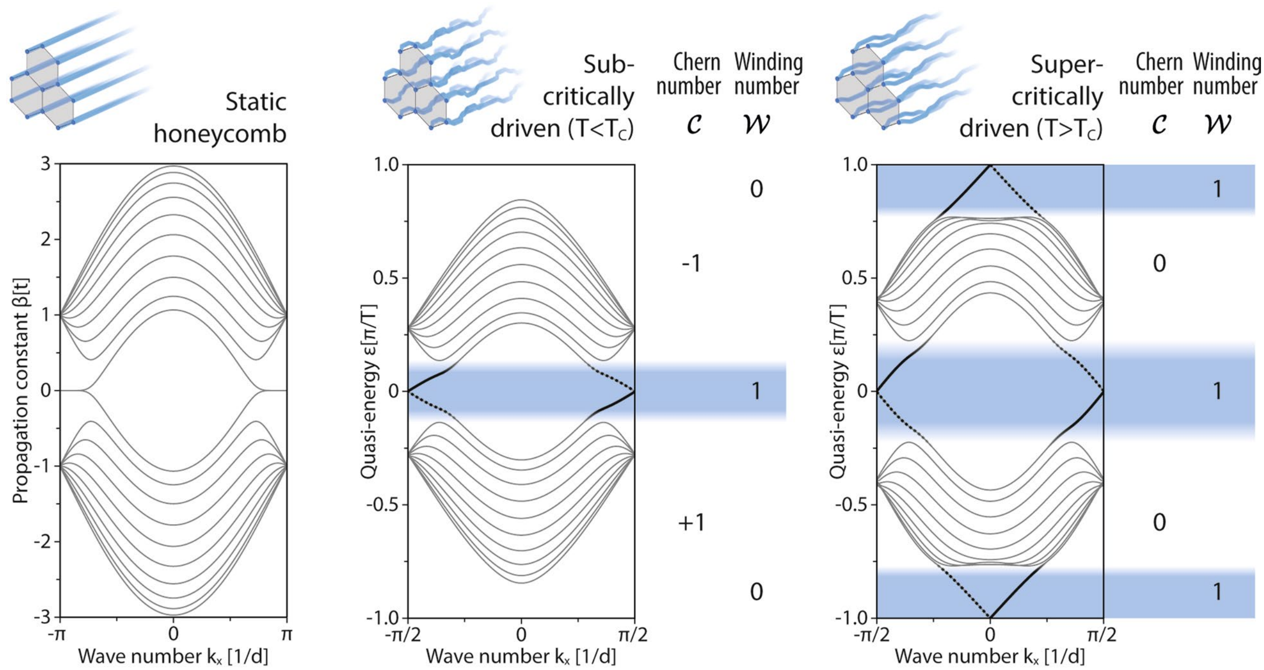

Extended Data Fig. 2 | Honeycomb helical FTI. A driven honeycomb lattice with sinusoidally modulated time-periodic coupling terms exhibits a secondary topological phase in response to an increase of the driving period. At the critical driving period $T_C = \pi/3$ the gap at the Floquet zone collapses and reopens with a topologically non-trivial winding number. This corresponds to an anomalous phase with a trivial Chern number, signifying a topological phase transition.

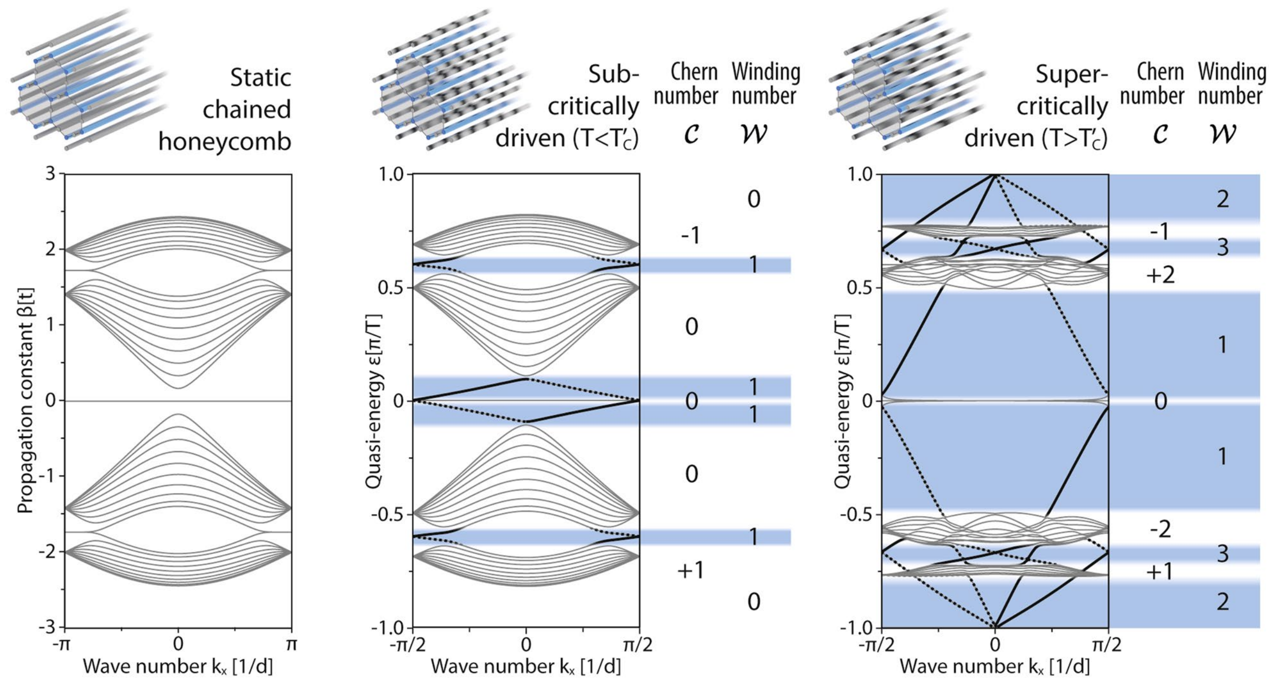

Extended Data Fig. 3 | Chained honeycomb FTI. Above its critical modulation period $T'_C = \pi$, the chain-driven honeycomb lattice enters a secondary topological phase characterized by the band diagram shown on the right. In this configuration, the bands manifest a non-trivial topological structure characterized by higher order Chern invariants ($\mathcal{C} = 2$), and, in turn, the Chern gaps host an increased number of unidirectional edge states. Details on the modal amplitudes and propagation dynamics of the Chern states in the $\mathcal{C} = 2$ phase are provided in Supplementary Fig. 5.

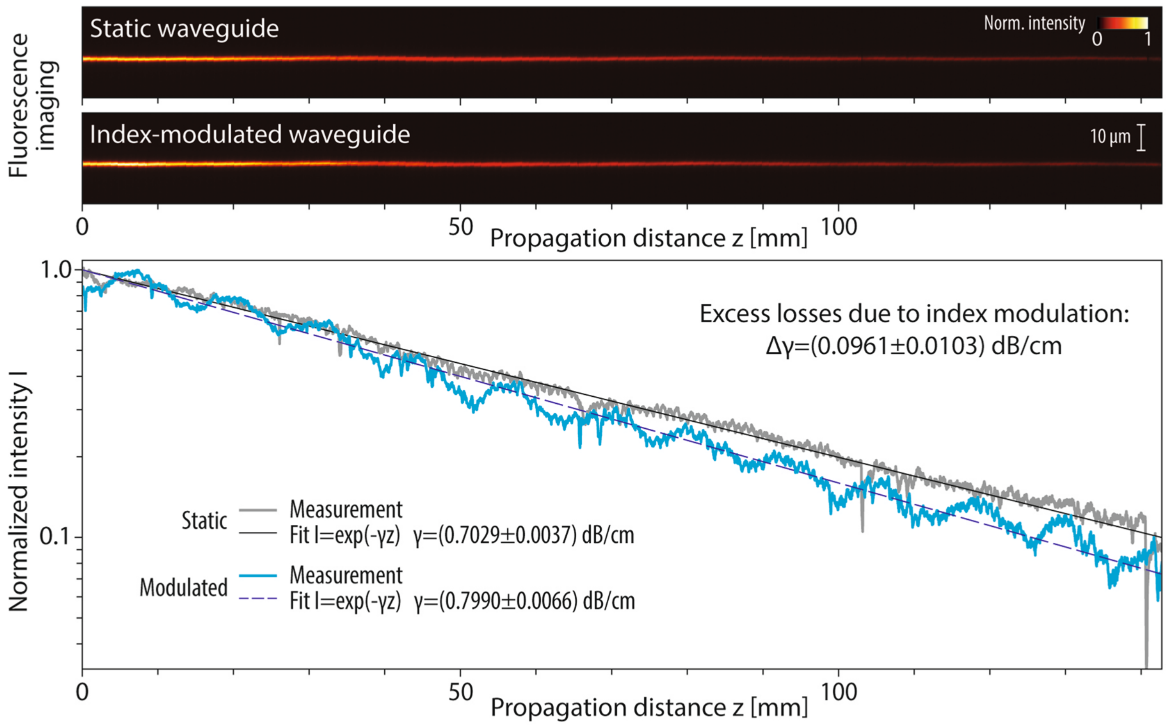

Extended Data Fig. 4 | Losses in index-modulated waveguides. Waveguide fluorescence[40] characterization confirms that even coarsely discretized index modulation (twelve constant-index segments approximating the ideal cosine Floquet cycle) only introduces excess losses of (0.096 ± 0.010)dB/cm relative to a straight constant-index waveguide. With half of the lattice sites being modulated, the mean excess losses of the bimorphic FTI are (0.048 ± 0.005)dB/cm, substantially below the value of 1.7 dB/cm reported for bending losses in conventional FTIs based on helically modulated waveguides[4]. Note that the apparent oscillations in the normalized intensity of the modulated waveguide are due to the different concentration of color centers formed at different writing speeds, resulting in a modulation of the fluorescence efficiency between the individual segments of each modulation period. Due to the large number of periods, this oscillation does not notably impact the measurement of the loss coefficient γ. The fluorescence itself is a feature of femtosecond laser-written waveguides in fused silica, and does not pose a substantial source of propagation losses[40].

nature portfolio

Corresponding author(s): Dr. Demetrios Christodoulides

Last updated by author(s): Mar 14, 2022

Reporting Summary

Nature Portfolio wishes to improve the reproducibility of the work that we publish. This form provides structure for consistency and transparency in reporting. For further information on Nature Portfolio policies, see our Editorial Policies and the Editorial Policy Checklist.

Statistics

For all statistical analyses, confirm that the following items are present in the figure legend, table legend, main text, or Methods section.

n/a	Confirmed	
☒	☐	The exact sample size (n) for each experimental group/condition, given as a discrete number and unit of measurement
☒	☐	A statement on whether measurements were taken from distinct samples or whether the same sample was measured repeatedly
☒	☐	The statistical test(s) used AND whether they are one- or two-sided *Only common tests should be described solely by name; describe more complex techniques in the Methods section.*
☒	☐	A description of all covariates tested
☒	☐	A description of any assumptions or corrections, such as tests of normality and adjustment for multiple comparisons
☒	☐	A full description of the statistical parameters including central tendency (e.g. means) or other basic estimates (e.g. regression coefficient) AND variation (e.g. standard deviation) or associated estimates of uncertainty (e.g. confidence intervals)
☒	☐	For null hypothesis testing, the test statistic (e.g. F, t, r) with confidence intervals, effect sizes, degrees of freedom and P value noted *Give P values as exact values whenever suitable.*
☒	☐	For Bayesian analysis, information on the choice of priors and Markov chain Monte Carlo settings
☒	☐	For hierarchical and complex designs, identification of the appropriate level for tests and full reporting of outcomes
☒	☐	Estimates of effect sizes (e.g. Cohen's d, Pearson's r), indicating how they were calculated

Our web collection on statistics for biologists contains articles on many of the points above.

Software and code

Policy information about availability of computer code

Data collection	The exerimental data (output intensity distributions) shown in this work were collected with a resolution of 12bit via standard LabView image acquisition routines.
Data analysis	Using Matlab, the recorded images were normalized to their respective peak values and subsequently exported as PNG files (8bit color map).

For manuscripts utilizing custom algorithms or software that are central to the research but not yet described in published literature, software must be made available to editors and reviewers. We strongly encourage code deposition in a community repository (e.g. GitHub). See the Nature Portfolio guidelines for submitting code & software for further information.

Data

Policy information about availability of data

All manuscripts must include a data availability statement. This statement should provide the following information, where applicable:

- Accession codes, unique identifiers, or web links for publicly available datasets
- A description of any restrictions on data availability
- For clinical datasets or third party data, please ensure that the statement adheres to our policy

The experimental data used to generate the figures in main manuscript and supplementary are available from the authors upon reasonable request.

Field-specific reporting

Please select the one below that is the best fit for your research. If you are not sure, read the appropriate sections before making your selection.

☐ Life sciences ☐ Behavioural & social sciences ☐ Ecological, evolutionary & environmental sciences

For a reference copy of the document with all sections, see nature.com/documents/nr-reporting-summary-flat.pdf

Life sciences study design

All studies must disclose on these points even when the disclosure is negative.

Sample size	*Describe how sample size was determined, detailing any statistical methods used to predetermine sample size OR if no sample-size calculation was performed, describe how sample sizes were chosen and provide a rationale for why these sample sizes are sufficient.*
Data exclusions	*Describe any data exclusions. If no data were excluded from the analyses, state so OR if data were excluded, describe the exclusions and the rationale behind them, indicating whether exclusion criteria were pre-established.*
Replication	*Describe the measures taken to verify the reproducibility of the experimental findings. If all attempts at replication were successful, confirm this OR if there are any findings that were not replicated or cannot be reproduced, note this and describe why.*
Randomization	*Describe how samples/organisms/participants were allocated into experimental groups. If allocation was not random, describe how covariates were controlled OR if this is not relevant to your study, explain why.*
Blinding	*Describe whether the investigators were blinded to group allocation during data collection and/or analysis. If blinding was not possible, describe why OR explain why blinding was not relevant to your study.*

Behavioural & social sciences study design

All studies must disclose on these points even when the disclosure is negative.

Study description	*Briefly describe the study type including whether data are quantitative, qualitative, or mixed-methods (e.g. qualitative cross-sectional, quantitative experimental, mixed-methods case study).*
Research sample	*State the research sample (e.g. Harvard university undergraduates, villagers in rural India) and provide relevant demographic information (e.g. age, sex) and indicate whether the sample is representative. Provide a rationale for the study sample chosen. For studies involving existing datasets, please describe the dataset and source.*
Sampling strategy	*Describe the sampling procedure (e.g. random, snowball, stratified, convenience). Describe the statistical methods that were used to predetermine sample size OR if no sample-size calculation was performed, describe how sample sizes were chosen and provide a rationale for why these sample sizes are sufficient. For qualitative data, please indicate whether data saturation was considered, and what criteria were used to decide that no further sampling was needed.*
Data collection	*Provide details about the data collection procedure, including the instruments or devices used to record the data (e.g. pen and paper, computer, eye tracker, video or audio equipment) whether anyone was present besides the participant(s) and the researcher, and whether the researcher was blind to experimental condition and/or the study hypothesis during data collection.*
Timing	*Indicate the start and stop dates of data collection. If there is a gap between collection periods, state the dates for each sample cohort.*
Data exclusions	*If no data were excluded from the analyses, state so OR if data were excluded, provide the exact number of exclusions and the rationale behind them, indicating whether exclusion criteria were pre-established.*
Non-participation	*State how many participants dropped out/declined participation and the reason(s) given OR provide response rate OR state that no participants dropped out/declined participation.*
Randomization	*If participants were not allocated into experimental groups, state so OR describe how participants were allocated to groups, and if allocation was not random, describe how covariates were controlled.*

Ecological, evolutionary & environmental sciences study design

All studies must disclose on these points even when the disclosure is negative.

Study description	*Briefly describe the study. For quantitative data include treatment factors and interactions, design structure (e.g. factorial, nested, hierarchical), nature and number of experimental units and replicates.*
Research sample	*Describe the research sample (e.g. a group of tagged Passer domesticus, all Stenocereus thurberi within Organ Pipe Cactus National*

Research sample	*Monument), and provide a rationale for the sample choice. When relevant, describe the organism taxa, source, sex, age range and any manipulations. State what population the sample is meant to represent when applicable. For studies involving existing datasets, describe the data and its source.*
Sampling strategy	*Note the sampling procedure. Describe the statistical methods that were used to predetermine sample size OR if no sample-size calculation was performed, describe how sample sizes were chosen and provide a rationale for why these sample sizes are sufficient.*
Data collection	*Describe the data collection procedure, including who recorded the data and how.*
Timing and spatial scale	*Indicate the start and stop dates of data collection, noting the frequency and periodicity of sampling and providing a rationale for these choices. If there is a gap between collection periods, state the dates for each sample cohort. Specify the spatial scale from which the data are taken*
Data exclusions	*If no data were excluded from the analyses, state so OR if data were excluded, describe the exclusions and the rationale behind them, indicating whether exclusion criteria were pre-established.*
Reproducibility	*Describe the measures taken to verify the reproducibility of experimental findings. For each experiment, note whether any attempts to repeat the experiment failed OR state that all attempts to repeat the experiment were successful.*
Randomization	*Describe how samples/organisms/participants were allocated into groups. If allocation was not random, describe how covariates were controlled. If this is not relevant to your study, explain why.*
Blinding	*Describe the extent of blinding used during data acquisition and analysis. If blinding was not possible, describe why OR explain why blinding was not relevant to your study.*

Did the study involve field work? ☐ Yes ☒ No

Reporting for specific materials, systems and methods

We require information from authors about some types of materials, experimental systems and methods used in many studies. Here, indicate whether each material, system or method listed is relevant to your study. If you are not sure if a list item applies to your research, read the appropriate section before selecting a response.

Materials & experimental systems

n/a	Involved in the study
☒	☐ Antibodies
☒	☐ Eukaryotic cell lines
☒	☐ Palaeontology and archaeology
☒	☐ Animals and other organisms
☒	☐ Human research participants
☒	☐ Clinical data
☒	☐ Dual use research of concern

Methods

n/a	Involved in the study
☒	☐ ChIP-seq
☒	☐ Flow cytometry
☒	☐ MRI-based neuroimaging